INSTITUTE OF PHYSICS PUBLISHING PHYSICS IN MEDICINE AND BIOLOGY

Phys. Med. Biol. **50** (2005) 4409–4428 doi:10.1088/0031-9155/50/18/011

In vitro measurements of absolute blood oxygen saturation using pulsed near-infrared photoacoustic spectroscopy: accuracy and resolution

Jan Laufer, Clare Elwell, Dave Delpy and Paul Beard

Department of Medical Physics and Bioengineering, University College London, Malet Place Engineering Building, London WC1E 6BT, UK

Received 19 May 2005, in final form 1 August 2005
Published 7 September 2005
Online at stacks.iop.org/PMB/50/4409

Abstract

Pulsed photoacoustic spectroscopy was used to measure blood oxygen saturation *in vitro*. An optical parametric oscillator laser system provided nanosecond excitation pulses over the wavelength range 740–1040 nm which were used to generate photoacoustic signals in a cuvette through which a saline suspension of red blood cells was circulated. The signal amplitude and the effective attenuation coefficient were extracted from the photoacoustic signals as a function of wavelength to provide photoacoustic spectra of the blood. From these, the relative concentrations of oxy- and deoxyhaemoglobin, and therefore blood oxygen saturation (SO_2), were determined using forward models of the absorbed energy distribution based on diffusion theory. A standard linear model of the dependence of absorbance on the concentration of chromophores was also used to calculate the blood oxygen saturation from the signal amplitude spectra. The diffusion approximation model was shown to produce the highest accuracy in blood SO_2. The photoacoustically determined oxygen saturation was found to have an accuracy of $\pm 4\%$ SO_2 for signal amplitude data and $\pm 2.5\%$ SO_2 for effective attenuation spectra. The smallest change in oxygen saturation that can be measured using this technique was $\pm 1\%$ SO_2.

1. Introduction

Biomedical photoacoustic techniques are based upon the generation of broadband (tens of MHz) ultrasonic waves by the absorption of short pulses of laser light in tissues. The time history of the acoustic waves detected by an ultrasound transducer on the tissue surface provides a measure of the spatial distribution of the absorbed optical energy distribution, which in turn is a function of the tissue optical properties. By varying the excitation laser wavelength, spatially resolved spectroscopic information can therefore be obtained by analysing the amplitude and temporal characteristics of the signals recorded at different wavelengths. This offers the prospect of quantifying the concentration of specific localized chromophores in tissues by

comparing their known spectral signatures with spectroscopic photoacoustic measurements obtained in this way. A physiologically important example is the measurement of regional variations of absolute blood oxygen saturation (SO_2) using the well-known specific absorption spectra of oxy- (HbO_2) and deoxyhaemoglobin (HHb) (Cope 1991) at near-infrared (NIR) wavelengths. Ultimately, by combining this spectroscopic capability with photoacoustic imaging methods (Beard 2002, Wang *et al* 2003, Kolkman *et al* 2003), the technique offers the prospect of providing high resolution three-dimensional maps of oxygenation over the vasculature non-invasively. This would have many important applications such as the study of oxygenation heterogeneity in tumours and other abnormalities characterized by changes in tissue oxygenation or perfusion status. However, if this ambitious objective is to be realized, a rigorous and experimentally validated methodology for recovering values of SO_2 from the spectroscopic photoacoustic signals is required. The first step in this endeavour is to develop and validate methods of obtaining SO_2 under the simplest and most well-controlled experimental conditions possible. This is most obviously achieved by making measurements in a cuvette in order to avoid the confounding influence of the physiological environment, the blood vessel geometry, surrounding tissues and so on. Although several *in vitro* studies of this nature have previously been undertaken, most have been limited to demonstrating that the wavelength dependence of specific characteristics of photoacoustic signals generated are in qualitative agreement with the known SO_2-dependent absorption spectrum of blood and have fallen short of recovering absolute SO_2 values from the measurements (Fainchtein *et al* 2000, Esenaliev *et al* 2002, Savateeva *et al* 2002). Attempts at the *in vivo* measurement of absolute (Paltauf *et al* 2001) and relative (Wang *et al* 2004) blood SO_2 have been made but in the absence of either an independent measurement or a validated methodology they are, at best, of uncertain accuracy.

The purpose of this study is to address these limitations by expanding upon a previous preliminary investigation into the photoacoustic measurement of absolute blood SO_2 (Laufer *et al* 2004). In the current paper, a comprehensive description of the theoretical framework and methodology for recovering absolute blood SO_2 values and their uncertainties from spectroscopic photoacoustic signals is provided. This methodology is then applied to experimentally measured photoacoustic spectra obtained in a cuvette of blood of various oxygenation levels and the resulting photoacoustically determined SO_2 values compared to those obtained with a CO-oximeter to determine the accuracy of the technique.

In this paper, section 2 provides an overview of the photoacoustic measurement of blood SO_2. Sections 3 and 4 describe a model of the photoacoustic signal generation process and section 5 discusses the use of this model for recovering SO_2 from measured photoacoustic spectra. Section 6 describes the experimental set-up used and section 7 the accuracy and resolution of the SO_2 values obtained from the photoacoustic measurements. Section 8 contains the discussion and conclusion.

2. Photoacoustic measurement of blood oxygenation: overview

The photoacoustic measurement of blood oxygen saturation is based upon the assumption that the amplitude and temporal characteristics of the detected photoacoustic signal are dependent upon the optical properties of blood. By extracting a parameter or data type from the signal that is representative of these characteristics and plotting it against wavelength, a measured photoacoustic spectrum can be formed. Sections 3–5 describe the steps required to recover blood SO_2 from these spectra. Firstly, a model that describes the time dependent photoacoustic signal as a function of the optical properties of blood is formulated. This comprises a simple and well-established one-dimensional model that relates the acoustic pressure as a function of

time to the axial distribution of absorbed laser energy (section 3), the latter being described by a modified version of diffusion theory (section 4). Secondly, this model is used to formulate the relationship between a specific data type extracted from the photoacoustic signal and the known wavelength dependent specific absorption coefficients of oxy- and deoxyhaemoglobin, and their relative concentrations, c_{HbO2} and c_{HHb} respectively. Termed the forward model, it provides a means of generating theoretical photoacoustic spectra which can then be fitted to the measured photoacoustic spectrum by adjusting the model input parameters $c_{\mathrm{HbO_2}}$ and c_{HHb}. The values that yield the best fit are then used to calculate SO_2 using

$$SO_2 = \frac{c_{\mathrm{HbO_2}}}{c_{\mathrm{HbO_2}} + c_{\mathrm{HHb}}} \times 100\%. \tag{1}$$

In this study, the use of two different data types was investigated: the peak amplitude of the photoacoustic signal and the effective attenuation coefficient, which is recovered from the temporal characteristics of the signal. Section 5 describes the forward models developed for each of these data types, the computational means by which they were used to obtain SO_2 and the methods used to estimate the accuracy and resolution of the measurement.

3. Photoacoustic signal generation

The photoacoustic measurement geometry used in this study is depicted in figure 1(a). A large diameter collimated pulsed laser beam is incident on an optically transparent cuvette through which blood was circulated. The absorption of the laser pulse in the blood creates a localized temperature rise and subsequent rapid thermal expansion, which produces a sudden increase in pressure. Assuming impulsive heating and therefore thermal and stress confinement, the initial axial pressure distribution, $P(z, \mu_a, \mu_s)$, mirrors the depth dependent spatial profile of the absorbed optical energy (figure 1(b)) and is given by

$$P(z, \mu_a, \mu_s) = \Gamma \mu_a \Phi_0 \Phi(z, \mu_a, \mu_s) \tag{2}$$

where Γ is the dimensionless Grüneisen coefficient, a measure of the conversion efficiency of thermal energy to stress. Φ_0 is the fluence at the surface, $\Phi(z, \mu_a, \mu_s)$ is the normalized fluence distribution as a function of depth z and μ_a and μ_s are the absorption and scattering coefficients respectively of blood.

This initial pressure distribution acts as a source of acoustic energy that emits a broadband ultrasound pulse that propagates away at the speed of sound and is detected by an acoustic detector situated on the opposite side of the cuvette. The time profile of the initial compressive part of the detected photoacoustic signal, $S(t)$ (figure 1(c)) is a direct representation of $P(z, \mu_a, \mu_s)$. Thus by converting the distance z to time t using the speed of sound c_s, $S(t)$ can be written as:

$$S(t) = K \mu_a \Phi(c_s(t_0 - t), \mu_a, \mu_s) \tag{3}$$

where t_0 is the acoustic transit time between the illuminated surface at $z = 0$ and the detector. K is a system response constant, which depends on the incident fluence, detector sensitivity, acoustic attenuation and Γ. In order to complete equation (3) and express it explicitly as a function of μ_a, an expression for the fluence term $\Phi(z, \mu_a, \mu_s)$ in equation (2) is required. This requires the use of a model of light transport in blood as described in the following section.

4. Modelling the light transport in blood

The optical properties of the leucocyte depleted blood samples measured in this study were determined by the red blood cells and the plasma. Both contain predominately water, which is

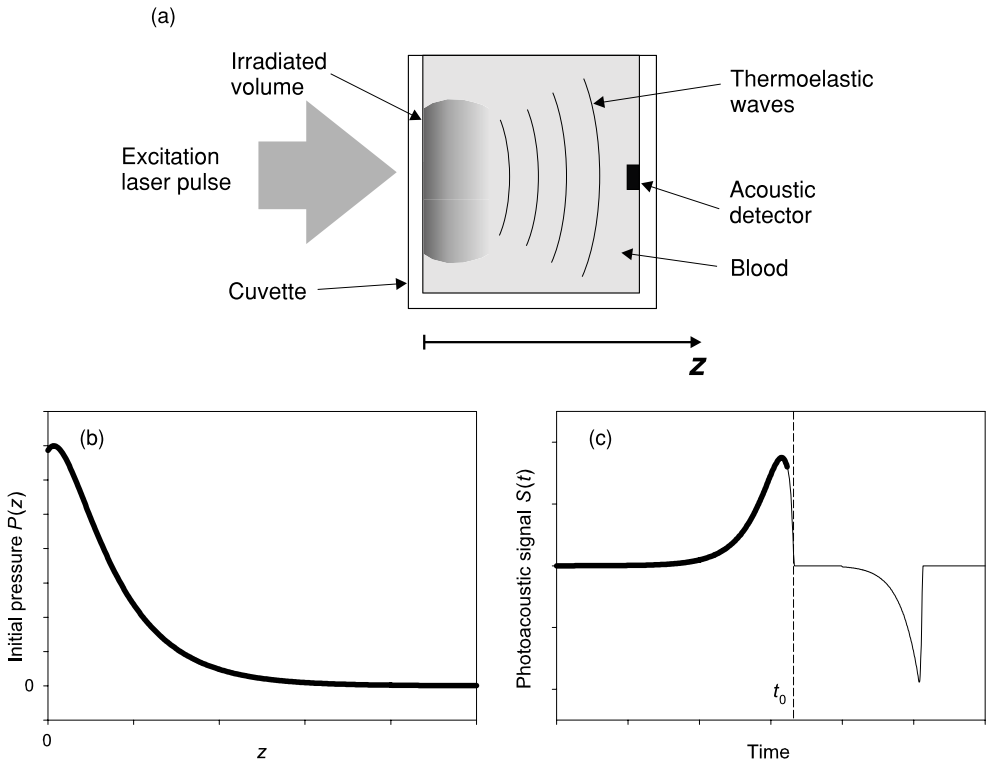

Figure 1. (a) Schematic of the photoacoustic generation and detection geometry, (b) the initial axial pressure distribution, which is proportional to the absorbed optical energy distribution and (c) the resulting detected photoacoustic signal $S(t)$. The initial compressive part of $S(t)$ (indicated by the bold line) is the plane wave component of the signal and corresponds to the initial pressure distribution shown in (b). Thus, the positive peak represents the absorbed energy close to the surface. The negative part of the signal is the time-delayed edge wave component originating from the perimeter of the excitation beam. It is assumed that the cuvette wall and the surrounding medium are well matched to the blood to avoid reflections.

one of the main absorbers in tissue. The other absorber is haemoglobin in its two most common forms of oxy- and deoxyhaemoglobin, which is contained in the red blood cells. Although other forms of haemoglobin such as carboxy- and methaemoglobin are also present, their contribution to the total attenuation can be neglected since they exhibit very low absorption coefficients in the near-infrared wavelength region and are normally only present at low concentrations. Due to the presence of haemoglobin, the intracellular fluid of red blood cells has a higher refractive index than the plasma and this causes optical scattering. The total optical attenuation in blood is therefore principally a combination of the absorption by HHb, HbO_2 and water, and optical scattering as illustrated in figure 2.

To describe the depth dependent fluence distribution $\Phi(z, \mu_a, \mu_s)$ in equation (2), a model of the light transport in blood therefore needs to incorporate the effects of absorption and scattering. In this study, an analytic solution (equation (A.6) in the appendix) to the diffusion equation for a large diameter collimated incident beam illuminating an infinite half space slab of homogeneous turbid media was used. Termed the δ-E(3) diffusion model, this incorporates the so-called delta-Eddington approximation in order to improve the description of the light transport at shallow depths where standard diffusion theory is of limited accuracy—

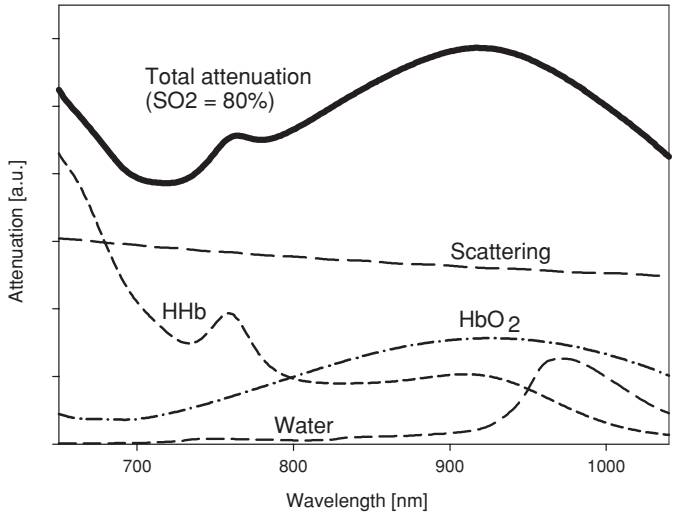

Figure 2. The total optical attenuation in blood is determined by the absorption by HHb, HbO_2, and water and the scattering caused by the refractive index mismatch between the red blood cells and the plasma. An example of the total attenuation for a blood SO_2 of 80% is shown by the bold line.

a necessary step since one of the data types to be extracted from the detected photoacoustic signal is the peak amplitude which corresponds to the absorbed optical energy close to the surface. For greater depths, equation (A.6) reduces to the simple exponential function, with decay constant μ_{eff}, given by equation (A.10). This expression is used in equation (3) to describe the part of the photoacoustic signal from which μ_{eff}, the second data type, is obtained as discussed in section 5.2.

5. Determination of blood SO_2 from measured photoacoustic spectra

Two types of measured photoacoustic spectra are considered in this study. The first is termed the relative photoacoustic amplitude spectrum and is obtained by plotting the variation of the peak amplitude of the photoacoustic signal with wavelength. The second is termed the absolute μ_{eff} spectrum and is obtained by plotting the absolute value of μ_{eff} recovered from the shape of the photoacoustic signal as a function of wavelength. In order to extract blood SO_2 from both types of measured spectra, forward models based upon equation (3) that describe the wavelength dependence of both data types have been formulated. The following sections describe these models and how they were used to calculate SO_2.

5.1. Relative photoacoustic amplitude spectrum

Two methods of extracting SO_2 from the measured photoacoustic amplitude spectrum are described. The first, method 1, iteratively fits a nonlinear forward model of the photoacoustic amplitude spectrum to the measured spectrum—its distinguishing feature being that it incorporates the δ-E(3) diffusion model of light transport referred to in section 4. The values of c_{HbO_2} and c_{HHb} that correspond to the best fit are then used in equation (1) to determine SO_2. The second approach, method 2, employs a linear forward model which assumes that the photoacoustic signal amplitude is directly proportional to the absorption coefficient. SO_2

is then obtained by forming a set of simultaneous equations (one for each wavelength) and solving for c_{HbO2} and c_{HHb} using standard linear algebraic methods.

5.1.1. Method I: δ-E(3) diffusion model. The forward model of the photoacoustic amplitude spectrum is

$$A(\lambda) = \max(S(t, \mu_a(\lambda), \mu_s(\lambda))), \tag{4}$$

where $\mu_a(\lambda)$ and $\mu_s(\lambda)$ are the wavelength dependent absorption and scattering coefficients respectively and max denotes the peak amplitude of the photoacoustic waveform $S(t, \mu_a(\lambda), \mu_s(\lambda))$. The latter, now written explicitly as a function of wavelength, is given by equation (3) with the fluence term obtained from equation (A.6) in the appendix.

Absorption in blood at near-infrared wavelengths is assumed to be dominated by three chromophores: deoxyhaemoglobin, oxyhaemoglobin and water. Thus $\mu_a(\lambda)$ can be written as the linear sum of the individual absorption contributions by each chromophore:

$$\mu_a(\lambda) = \alpha_{HHb}(\lambda)c_{HHb} + \alpha_{HbO_2}(\lambda)c_{HbO_2} + \mu_{a\_water}(\lambda) \tag{5}$$

where $\alpha_{HHb}(\lambda)$ and $\alpha_{HbO_2}(\lambda)$ are the wavelength dependent specific absorption coefficients (units: mm^{-1} $molar^{-1}$, defined using the natural log) of deoxyhaemoglobin and oxyhaemoglobin respectively. These coefficients are known to be within ±1% (Cope 1991). $\mu_{a\_water}(\lambda)$ is the wavelength dependent absorption coefficient of water (Hale *et al* 1973) and was adjusted to take account of its concentration in blood which is approximately 80–85% for a haematocrit (the number of red blood cells per unit volume) of 45% (Geigy 1956). $\mu_s(\lambda)$ is written as follows:

$$\mu_s(\lambda) = \alpha_{scat}(\lambda)k \tag{6}$$

where $\alpha_{scat}(\lambda)$ is the scattering efficiency and represents the normalized scattering wavelength dependence. k is a wavelength independent constant appropriately scaled to represent the assumption that $\mu_s(\lambda)$ is linearly dependent on haematocrit over the physiological range (Roggan *et al* 1999) at NIR wavelengths. It is further assumed that the scattering anisotropy, g, is independent of changes in the haematocrit and is set to a constant value of 0.975 (Roggan *et al* 1999). $\alpha_{scat}(\lambda)$ can be obtained theoretically (e.g. from Mie theory) or by making measurements of $\mu_s(\lambda)$ or the reduced scattering coefficient, $\mu_s'(\lambda) = \mu_s(1 - g)$. In this study, $\mu_s'(\lambda)$ was obtained from photoacoustic measurements of $\mu_{eff}(\lambda)$ in blood of known $\mu_a(\lambda)$ as described in section 7.1.

Substituting equations (5) and (6) into equation (4) yields the forward model of the photoacoustic amplitude spectrum $A(\lambda)$ with known fixed input parameters $\alpha_{HHb}(\lambda)$, $\alpha_{HbO2}(\lambda)$, $\alpha_{scat}(\lambda)$ and g. The adjustable unknown parameters are c_{HHb}, c_{HbO2}, k and K. These are varied iteratively until the difference between the measured photoacoustic amplitude spectrum and that produced by the forward model is minimized. The values for c_{HHb} and c_{HbO2} corresponding to the best fit are then used in equation (1) to calculate SO_2. Since there are four unknown parameters in the forward model, a minimum of four photoacoustic waveforms detected at different wavelengths are required to obtain absolute values of c_{HHb} and c_{HbO2}. To determine SO_2, one less wavelength is required as the system response constant K cancels in equation (1).

To obtain an estimate of the uncertainty in the determined parameters based on the error in the measurement, the variance in c_{HHb} was calculated as follows:

$$\text{var}(c_{HHb}) = (X'X)^{-1}\sigma_{p-p}^2 \tag{7}$$

where X is the design matrix, the derivative of the model with respect to its variables, and σ_{p-p}^2 is the variance in the peak-to-peak amplitude for all measured wavelengths. The variance in

c_{HbO_2} was calculated similarly. The variances obtained in this way are determined solely by the variance of the amplitude measurements and do not include the effect of the uncertainties in the coefficients used in the model, such as the specific absorption coefficients and the scattering efficiency, since their influence on the final uncertainty in SO_2 was found to be insignificant. The uncertainty in SO_2 was calculated using equation (8) below:

$$\Delta SO_2 = \sqrt{\left(\frac{\Delta c_{HbO_2}}{c_{HbO_2}}\right)^2 + \left(\frac{\sqrt{\Delta c_{HbO_2}^2 + \Delta c_{HHb}^2}}{c_{HbO_2} + c_{HHb}}\right)^2} \frac{c_{HbO_2}}{c_{HbO_2} + c_{HHb}} \times 100\% \tag{8}$$

where Δc_{HHb} and Δc_{HbO_2} denote the standard deviation in c_{HHb} and c_{HbO_2} obtained from their corresponding variances. ΔSO_2 represents the smallest detectable change in SO_2 for a given standard deviation in the measurements.

5.1.2. Method II: linear model. Unlike the previous method which involved fitting a nonlinear forward model to the measured photoacoustic spectra, this approach employs a linear forward model, similar in form to those commonly used for conventional optical transmittance spectroscopy of non-scattering media composed of different chromophores (Cope 1991). In these, the total absorption is written as the sum of the absorption contributions by each chromophore, each contribution being linearly dependent upon chromophore concentration. Although the presence of scattering means that the photoacoustic signal amplitude is not strictly a linear function of μ_a, this type of model can provide acceptable accuracy if it is modified by assuming that the amplitude is proportional to the total attenuation $\mu_{tr} = \mu_a + \mu_s'$—that is to say the contribution to the total attenuation due to scattering is regarded as equivalent to that of an additional absorbing chromophore (Laufer *et al* 2004). The results in section 7 indicate that this assumption is reasonable for values of μ_a at NIR wavelengths for blood with a haematocrit and SO_2 within the physiological range and the photoacoustic source geometry used in this study. The wavelength dependent total attenuation in blood is then expressed as follows:

$$\mu_{tr}(\lambda) = \alpha_{HHb}(\lambda)c_{HHb} + \alpha_{HbO_2}(\lambda)c_{HbO_2} + \alpha_{scat}(\lambda)k' + \mu_{a\_water}(\lambda) \tag{9}$$

where the third term on the right-hand side represents the reduced scattering coefficient. This requires the constant in equation (6) to be re-defined as $k' = k(1 - g)$. Writing the photoacoustic amplitude spectrum as a linear function of μ_{tr}:

$$M_{p\text{–}p}(\lambda) = B\mu_{tr}(\lambda) \tag{10}$$

where $M_{p\text{–}p}(\lambda)$ is the wavelength dependent peak signal amplitude and B is a constant. Equation (10) can be written for each wavelength to form a set of linear equations, expressed in matrix notation as

$$M_{p\text{–}p} = AC \tag{11}$$

where $M_{p\text{–}p}$ is the $[n \times 1]$ vector of the peak signal amplitude measurements, where n is the number of wavelengths used. A is a $[n \times 4]$ matrix of $\alpha_{HHb}(\lambda)$, $\alpha_{HbO_2}(\lambda)$, $\alpha_{scat}(\lambda)$, and the absorption coefficient of water and C is the $[4 \times 1]$ vector of the relative concentrations. Unlike the nonlinear diffusion based model in section 5.1.1, we now have a linear system enabling C to be estimated directly using multilinear regression rather than iteratively to calculate c_{HHb}, c_{HbO_2}, k and B using

$$C = (A^T A)^{-1} A^T M_{p\text{–}p}, \tag{12}$$

where A^T denotes the transpose matrix of A. $(A^T A)^{-1} A^T$ is the so-called pseudo-inverse matrix of A. c_{HHb} and c_{HbO_2} are then substituted into equation (1) to calculate SO_2. As in the previous

section, measurements at a minimum of four different excitation wavelengths are required to determine c_{HHb}, $c_{\mathrm{HbO_2}}$, k, and B and three wavelengths to obtain SO_2. The variances in c_{HHb}, $c_{\mathrm{HbO_2}}$ and SO_2 are obtained in a similar manner to that outlined in section 5.1.1.

5.2. Absolute μ_{eff} spectrum

For depths greater than a few transport mean free paths, where the light has become fully diffuse, the axial fluence distribution and therefore the shape of the initial part of the photoacoustic signal is defined by the exponential function in equation (A.10) in the appendix. By fitting this equation to the initial compressive part of the photoacoustic signal, a value for the exponential constant μ_{eff} can be obtained. Since this is a function of $\mu_{\mathrm{a}}(\lambda)$, it provides an alternative data type to the peak amplitude used in section 5.1. The forward model for this data type is

$$\mu_{\mathrm{eff}}(\lambda) = \sqrt{3\mu_{\mathrm{a}}(\lambda)(\mu_{\mathrm{a}}(\lambda) + \mu_{\mathrm{s}}(\lambda)(1-g))}. \tag{13}$$

Equations (5) and (6) are substituted into equation (13) to express it in terms of the additive contributions of the individual chromophores and the scattering in blood. This allows the calculation of a theoretical μ_{eff} spectrum as a function of c_{HHb}, $c_{\mathrm{HbO_2}}$ and k, assuming fixed input parameters $\alpha_{\mathrm{HHb}}(\lambda)$, $\alpha_{\mathrm{HbO_2}}(\lambda)$, $\alpha_{\mathrm{scat}}(\lambda)$ and g. In order to determine c_{HHb} and $c_{\mathrm{HbO_2}}$, the difference between the spectrum of μ_{eff} provided by equation (13) and the spectrum obtained from the photoacoustic signals was iteratively minimized by varying c_{HHb}, $c_{\mathrm{HbO_2}}$ and k as in section 5.1.1—the inversion method in section 5.1.2 is not applicable since μ_{eff} is a nonlinear function of μ_{a}. The values for c_{HHb} and $c_{\mathrm{HbO_2}}$ corresponding to the best fit are then used to calculate SO_2 using equation (1). Unlike the methods outlined in section 5.1, the forward model of equation (13) does not involve a scaling factor. There is therefore one less unknown parameter and so measurements at only three wavelengths are required to obtain c_{HHb} and $c_{\mathrm{HbO_2}}$. The uncertainty in SO_2 was calculated from the uncertainty in the fitted μ_{eff} in a manner similar to that described in section 5.1.1. The advantage of using μ_{eff} as a data type is that, unlike the signal amplitude, it is independent of fluctuations in the incident fluence, detector sensitivity and other factors that make up the system response factor K. It is therefore an inherently more robust data type.

6. Methods and materials

6.1. Blood preparation

A total of ten leucocyte depleted blood samples, which had exceeded the expiry date of 30 days since donation, were obtained from the blood bank of the local hospital. Ethics approval had been granted for this study. 2000 units of heparin were added to 200 ml of blood, which was then centrifuged at 3000 rpm to separate the red blood cells from the plasma. The plasma was then removed and replaced with a phosphate-buffered saline solution (pH 7.4, Sigma Aldrich). This process was repeated four times to produce a saline suspension of red blood cells. The total haemoglobin concentration of the samples used for photoacoustic measurements was between 120 and 160 g l^{-1}.

6.2. Experimental set-up and methods

Figure 3 shows a diagram of the experimental set-up. A tuneable type I optical parametric oscillator (OPO) laser system (Spectra-Physics) provided 7 ns excitation pulses at wavelengths

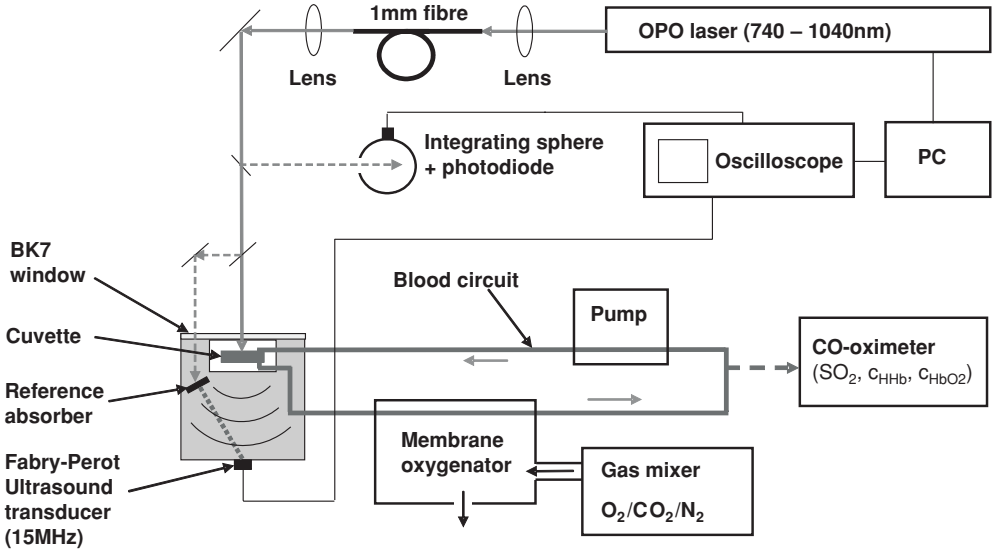

Figure 3. The experimental set-up for the measurement of photoacoustic signals generated in blood as a function of wavelength. A membrane oxygenator allowed the control of blood oxygenation and a CO-oximeter was used to make independent measurements of SO_2.

between 740 nm and 1040 nm. The output of the OPO was coupled into a 1 mm fused silica fibre to homogenize the beam and minimize the effects of the beam movement by the OPO during wavelength tuning. The output of the distal end of the fibre was imaged onto the cuvette to produce a beam diameter of approximately 5 mm. The incident fluence ranged from 30 to 40 mJ cm^{-2}. The cuvette provided a chamber of 7 mm depth and 15 mm diameter through which blood was circulated. The front window had a thickness of 5 mm which was fabricated from polymethylmethacrylate. The back window consisted of a 23 μm polymer film to ensure minimal attenuation of the photoacoustic waves. The cuvette was placed in a water bath to allow the propagation of the photoacoustic waves to an angle-tuned Fabry-Perot ultrasound transducer for detection (Beard *et al* 1999, Beard 2003). The transducer is based on the interferometric sensing of acoustically-induced changes in the optical thickness of a 75 μm polyethylene terephthalate film and has a broadband (15 MHz) detection sensitivity of 1.0 kPa. Long-term sensitivity drifts of the transducer were monitored by generating photoacoustic signals in a reference absorber using a small fraction of the incident excitation pulse. Variations in sensitivity were less than 10% over a measurement period of 8 h and therefore insignificant over the 20 min it took to complete a single wavelength scan.

A small portion of the incident beam was directed via a beamsplitter onto an integrating sphere where the intensity was measured with a reference photodiode. The photodiode output was captured simultaneously with a photoacoustic signal and later used to normalize the detected waveforms with respect to the incident pulse energy. The wavelength dependence of the photodiode sensitivity and the transmission spectra of the optical components between the beamsplitter and the surface of the blood (e.g. the perspex cuvette window) were accounted for in a single wavelength-dependent correction factor. This was obtained by simultaneously measuring the pulse energy transmitted through the cuvette window using a calibrated volume absorber power meter with a flat spectral response and the photodiode output.

The waveform acquisition and the wavelength tuning of the OPO were automated and controlled using LabView. The tuning range was between 740 nm and 1040 nm in steps of 10 nm with a tuning accuracy of better than 0.7 nm.

Blood at room temperature was continuously pumped through the cuvette and an extracorporeal membrane oxygenator (Lilliput 901, Dideco). A gas mixer was used to provide a constant air flow of O_2, N_2 and CO_2. Blood SO_2 was controlled by adjusting the ratio of O_2 and N_2. The amount of CO_2 in the circuit was held constant at 7%. At each blood SO_2 level, a photoacoustic spectrum was measured. The detected photoacoustic waveforms and the reference photodiode output were averaged over 60 acquisitions using a digital oscilloscope (TDS784D, Tektronix). Four such averaged waveforms were captured at each wavelength. Small samples of blood were taken from the circuit several times before and during the wavelength scan and analysed using a CO-oximeter (IL482, Instrumentation Laboratories Inc). The CO-oximeter measurements provided gold standard measurements for the total haemoglobin concentration (± 3.0 g l^{-1}), the haemoglobin fractions $\%HbO_2$ ($\pm 1\%$) and %HHb ($\pm 3\%$), and SO_2 ($\pm 4.1\%$) against which the photoacoustically measured SO_2 could be compared. The variation in SO_2 measured before and after a wavelength scan of typically 20 min duration was typically less than 1%. Photoacoustic spectra were obtained for a number of blood oxygen saturations ranging from 2% to 100% over the course of 6 to 8 h. Haemolysis, which is the destruction of red blood cells as a result of the circulation, was assessed by conducting a blood cell count of samples taken before and after the experiments. The difference in the cell counts was less than 0.5% allowing the effect of haemolysis to be neglected.

The linewidth of type I OPO laser systems is strongly dependent on emission wavelength varying from 2–3 nm FWHM at 1000 nm to 15–25 nm around 740 nm. This results in a smearing of spectral features such as the HHb absorption peak at 760 nm. To account for this, the wavelength-dependent linewidth was measured using a spectrometer and convolved with the known specific absorption spectra of HHb and HbO_2.

6.3. Analysis of the photoacoustic waveforms

Figure 4 shows a typical photoacoustic signal detected using the experimental set-up in figure 3. Unlike the illustrative example shown in figure 1(c), the positive plane wave and negative edge wave components of the signal are not temporally separated. This is because the relatively small diameter of the excitation laser beam compared to the source–detector distance of the experimental arrangement causes the two components to partially overlap. For this reason it is the peak–peak amplitude of the signal rather than the peak positive value that is assumed to be proportional to the maximum value of the absorbed energy and is used to represent the amplitude data type. The second parameter extracted from the signal is the effective attenuation coefficient, μ_{eff}, and is obtained by fitting equation (3) (using equation (A.10) in the appendix for the fluence term) to the early compressive part of the photoacoustic signal. To ensure that this corresponded to the part of the signal that had originated only from depths at which most of the light had become diffuse, the curve fit was performed only on data points that corresponded to depths greater than three transport mean free paths as indicated in figure 4.

Four waveforms captured at each wavelength were combined into an averaged waveform with a corresponding standard deviation. The corresponding photodiode measurements for each of the four waveforms were also averaged and multiplied by the spectral correction factor referred to in section 6.2. The standard deviations in the peak-to-peak amplitude and the correction factor were combined to give a total standard deviation for the photoacoustic

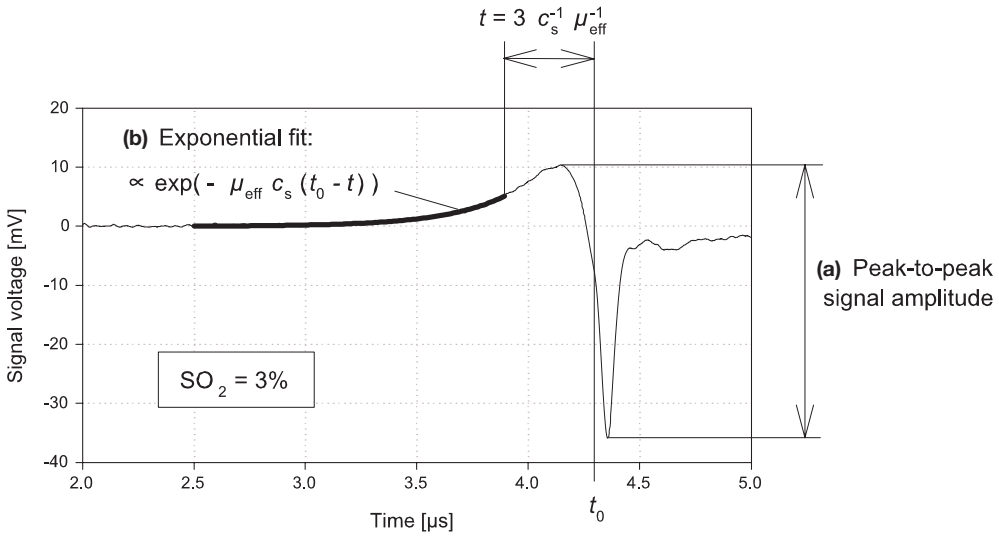

Figure 4. An example of a measured photoacoustic signal detected in blood at 740 nm using the experimental arrangement in figure 3. Two parameters were extracted from the signal: (a) the peak-to-peak amplitude and (b) the effective attenuation coefficient, μ_{eff}, obtained by fitting an exponential function to the initial compressive part of the photoacoustic wave (thick line).

signal amplitude measurement. The variance of the fitted μ_{eff}, a measure of its uncertainty, was calculated from the standard deviation of each data point of the photoacoustic signal according to equation (14) below:

$$\text{var}(\mu_{\text{eff}}) = (X'X)^{-1}\sigma^2 \tag{14}$$

where X is the design matrix, which contains the sensitivity of the model, in this case the exponential function, to μ_{eff} and the scaling factor. σ^2 is a $[n \times n]$ diagonal matrix of the variance, i.e. the square product of the standard deviation, of each of the n temporal data points of the photoacoustic signal to which the exponential function was fitted.

7. Experimental results

As shown in section 5, the forward models for each spectroscopic data type require the wavelength dependence of scattering $\alpha_{\text{scat}}(\lambda)$ to be included as a fixed input parameter. This was obtained photoacoustically as described in section 7.1. Examples of the measured amplitude and μ_{eff} photoacoustic spectra for different SO_2 values are provided in section 7.2 and the accuracy and resolution of the measurements of SO_2 obtained from each type of spectra are discussed in section 7.3.

7.1. Calculation of the wavelength dependence of scattering from photoacoustic spectra

As section 5 shows, the scattering wavelength dependence $\alpha_{\text{scat}}(\lambda)$ is required in order to measure SO_2. Assuming that g is wavelength independent over this limited range of wavelengths, $\alpha_{\text{scat}}(\lambda)$ can be obtained from the μ_s' spectrum. This can be obtained from a number of sources, such as Mie theory or published data. However, Mie theory is of limited accuracy in describing non-spherical scattering particles (Steinke and Shepherd 1988) while published μ_s' spectra (Roggan *et al* 1999, Enejder *et al* 2003) were found to either not cover

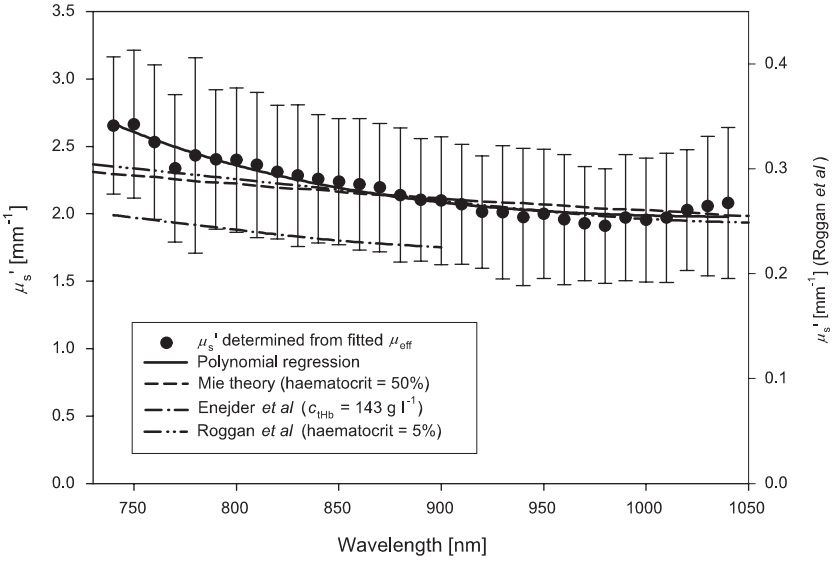

Figure 5. The wavelength dependence of the reduced scattering coefficient of blood determined from the photoacoustic μ_{eff} spectra. The polynomial regression through the data was used later to describe $\alpha_{scat}(\lambda)$. μ_s' spectra calculated using Mie theory and spectra measured by other groups are also shown for comparison.

the wavelength range of the photoacoustic measurements or to represent measurements on highly diluted blood, which may not be applicable to measurements on blood of physiological haematocrit.

For these reasons $\mu_s'(\lambda)$ was measured photoacoustically as follows. A set of 20 photoacoustic μ_{eff} spectra was obtained in blood at different SO_2 levels—the haematocrit for these measurements was in the physiological range of 40–50%. μ_{eff} was recovered from the photoacoustic signals as described in section 3.2 and $\mu_s'(\lambda)$ then obtained from $\mu_{eff}(\lambda)$ by re-arranging equation (13),

$$\mu_s'(\lambda) = \frac{\mu_{eff}^2(\lambda)}{3\mu_a(\lambda)} - \mu_a(\lambda) \tag{15}$$

where $\mu_a(\lambda)$ is given by equation (5) with $\alpha_{HHb}(\lambda)$, $\alpha_{HbO_2}(\lambda)$ and $\mu_{a\_water}(\lambda)$ known and c_{HHb} and c_{HbO_2} obtained from CO-oximeter measurements of the total haemoglobin concentration and SO_2. A total of 20 μ_s' spectra collected at different SO_2 were averaged. The result is shown in figure 5. For comparison purposes, spectra taken from published data are also shown together with a μ_s' spectrum calculated using Mie theory for a typical cell volume of 90 μm^3 (Bessman and Johnson 1975) and a dispersion approximation based on a study by Hammer *et al* (1998). The wavelength dependence as well as the absolute values of the μ_s' spectrum calculated from the photoacoustic μ_{eff} spectrum compares reasonably well with the results of Mie theory calculations and the published data. A polynomial function was fitted to the photoacoustically obtained μ_s' spectrum to provide an expression for $\alpha_{scat}(\lambda)$. This was used for the determination of SO_2 for all subsequently measured photoacoustic spectra. This provided more accurate results than those obtained using either the published μ_s' spectra or the predictions from Mie theory.

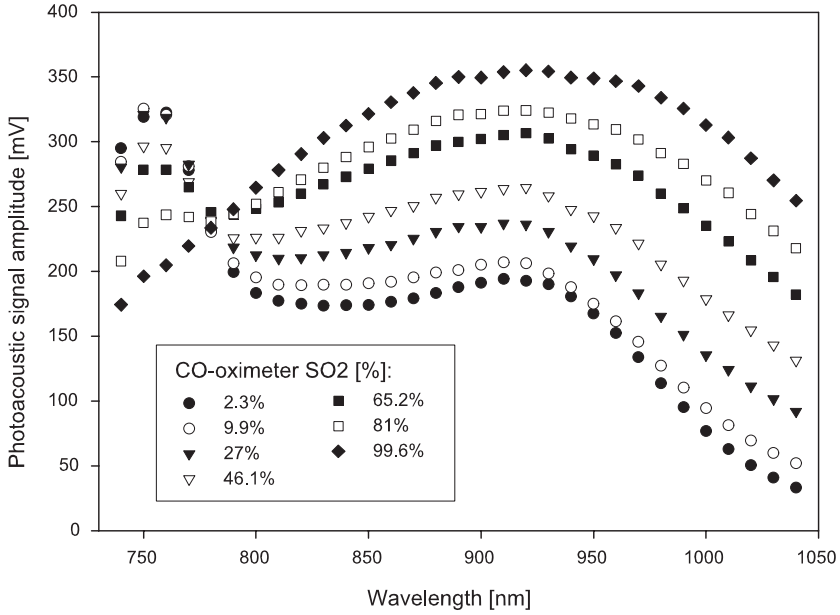

Figure 6. Photoacoustic amplitude spectra of blood at different oxygen saturations. Each data point has a standard deviation of less than ±1%.

7.2. Measured photoacoustic spectra as a function of SO_2

Figure 6 shows examples of the measured photoacoustic amplitude spectra for seven levels of blood SO_2 between 2.3% and 99.6%. A cursory inspection suggests these exhibit the well-known changes in the shape of the absorption spectrum of blood with SO_2. For example, the formation of the 760 nm peak as the blood becomes progressively more deoxygenated is clearly apparent. However, as figure 7 shows, if we directly compare the measured photoacoustic spectra for both amplitude and μ_{eff} data types for the two extremes of $SO_2 = 2.3\%$ and $SO_2 = 99.6\%$ against the known specific absorption spectra for these two SO_2 values, it is apparent that there are significant differences. This is principally due to the influence of scattering which is equivalent to adding a wavelength dependent dc offset and has the effect of flattening the spectrum. This can be seen in both the measured amplitude (figure 7(a)) and μ_{eff} spectra (figure 7(b)). The effect is greater for the latter because the initial compressive part of the photoacoustic waveform, from which μ_{eff} is obtained, originates from greater depths where the light has become diffuse and the influence of scattering is more significant. By contrast, the peak amplitude of the photoacoustic signal corresponds to the region immediately adjacent to the cuvette window where scattering has a relatively weak influence on the light distribution. If the effect of scattering is now incorporated by calculating the attenuation rather than absorption spectrum for the two SO_2 values using equation (10) (with $\alpha_{\text{scat}}(\lambda)$ obtained as described in section 7.1), we can see from figure 7(a) that the agreement with the measured amplitude spectra is significantly improved. Similarly, if we compare the measured μ_{eff} spectra with that calculated using equation (13), which includes scattering, the agreement is excellent (figure 7(b)). These results indicate that if the photoacoustic spectra of blood are to be related to the absorption spectra of c_{HHb} and c_{HbO_2} (the underlying principle behind the spectroscopic measurement of SO_2), the effect of scattering should be taken into account.

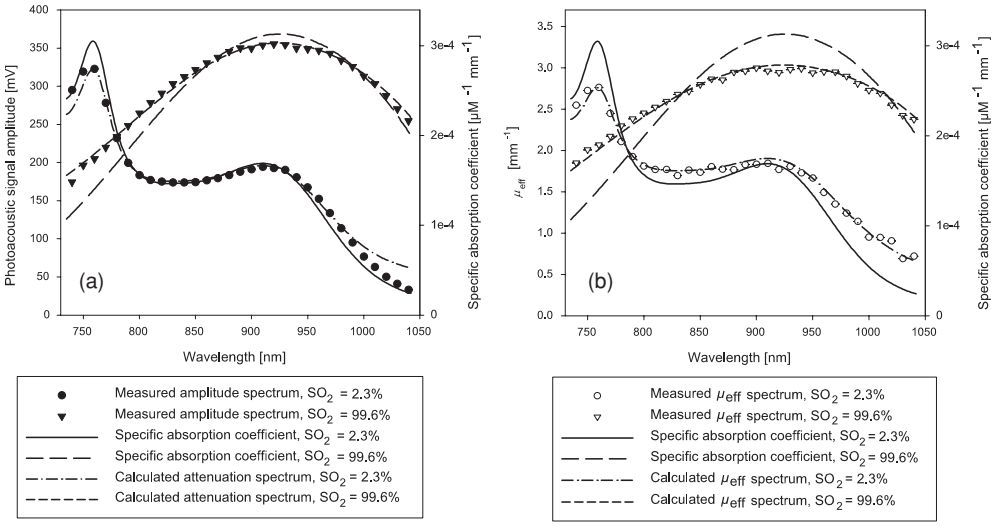

Figure 7. (a) Measured photoacoustic amplitude spectra compared to the specific absorption spectra and calculated attenuation spectra (obtained using equation (10)) of near fully oxygenated and deoxygenated blood. (b) Measured photoacoustic μ_{eff} spectra compared to the specific absorption spectra and calculated μ_{eff} spectra (obtained using equation (13)) also for near fully oxygenated and deoxygenated blood.

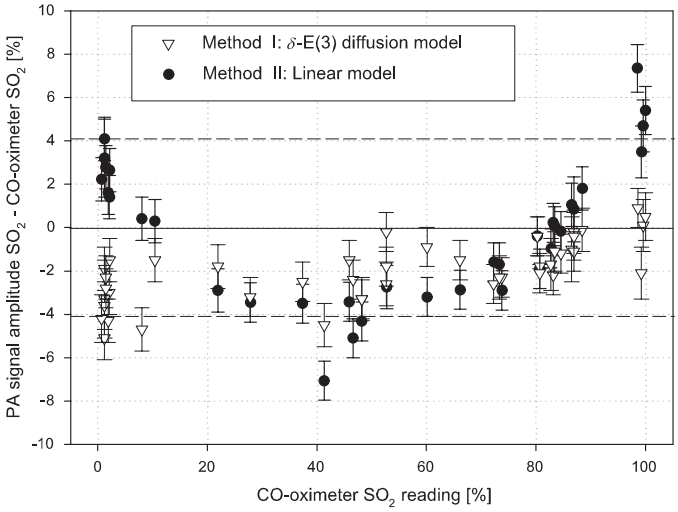

Figure 8. Bland-Altmann plot of the difference between the SO_2 determined from the photoacoustic (PA) amplitude spectra and the SO_2 measured by the CO-oximeter. The error bars indicate the uncertainty in the determined values. The horizontal dashed lines indicate the accuracy of the CO-oximeter measurements.

7.3. Photoacoustically determined SO_2 versus CO-oximeter SO_2

The Bland–Altmann plot in figure 8 shows the difference between SO_2 obtained from the measured photoacoustic signal amplitude spectra (using the δ-E(3) diffusion and linear models in section 5.1) and that measured using the CO-oximeter. A similar plot is shown in figure 9

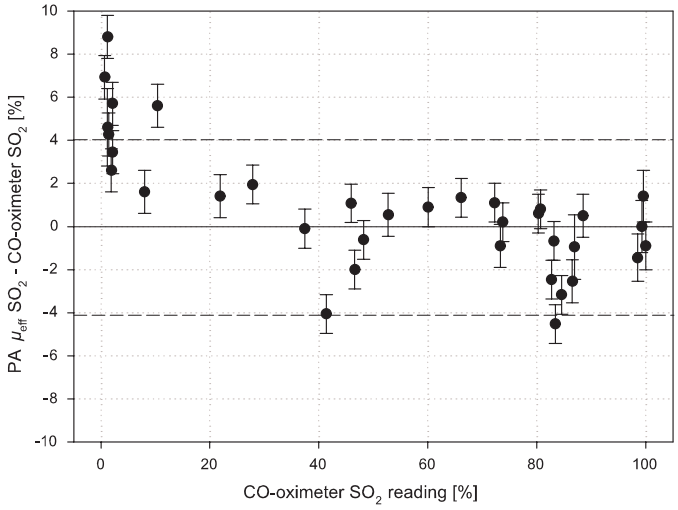

Figure 9. Bland–Altmann plot of the difference between the SO_2 calculated from the photoacoustic (PA) μ_{eff} spectra and the SO_2 measured by the CO-oximeter. The error bars indicate the uncertainty in the determined values. The horizontal dashed lines indicate the accuracy of the CO-oximeter.

for the SO_2 values obtained from the μ_{eff} spectra. Both types of spectra were obtained from the same set of photoacoustic signals to enable comparisons between the values of SO_2 obtained from each spectra to be made.

Figure 8 shows that the photoacoustically determined SO_2 values using method 1 and 2 are generally in close agreement with the CO-oximeter measurements with the majority of the measurements lying within the accuracy of the CO-oximeter as quoted by the manufacturer. The photoacoustic measurements using method 1 do, however, exhibit a small systematic under-reading of approximately 4% for SO_2 values between 5% and 50% and around 2% for $SO_2 > 50\%$. The data obtained using method 2 show a comparable, if slightly higher and more variable, systematic error over much this range. Such systematic errors are not observed in the μ_{eff} based measurements (figure 9). This suggests they may be due to inaccuracies in the wavelength dependent calibration factors which are used to correct only the amplitude spectra. Another suspected source of error is due to changes in the diameter of the excitation beam emerging from the optical fibre as a result of shifts in the OPO output beam as it tunes. This would cause the incident fluence to vary during wavelength tuning, corrupting the amplitude spectra, although not the μ_{eff} spectra. The generally lower accuracy obtained using method 2 is most likely due to limitations of the model which assumes that the signal amplitude is a linear function of μ_{tr}. For $SO_2 < 4\%$, all the measurements in both figures 8 and 9 show significant deviation from the CO-oximeter values. This may be a consequence of inaccuracies in the specific extinction spectrum of deoxyhaemoglobin due to the difficulty in obtaining truly fully deoxygenated haemoglobin—indeed the latter may have contributed directly to the inaccuracies in the data at low SO_2. The variation in the published specific absorption coefficient spectra illustrates this point (Horecker 1943, Barlow and Polanyi 1962, Takatani and Graham 1979, Wray *et al* 1988, Cope 1991). The resolution or the smallest change in SO_2 that can be measured is given by the error bars which represent the uncertainty in the measurement and is approximately $\pm 1\%$ for both the method 1 and method 2 based data over the whole SO_2 range.

The accuracy of the SO_2 values obtained from the μ_{eff} spectra shown in figure 9 is $\pm 2.5\%$ of the co-oximeter values (excluding the data for $SO_2 < 4\%$). The under-reading of the amplitude based measurements in figure 8 is not in evidence for these measurements. The improved accuracy is due to the more robust nature of μ_{eff} as a data type which, unlike amplitude, is independent of fluctuations in laser pulse energy, detector sensitivity and other scaling parameters. The resolution of the μ_{eff} based measurements in figure 9 is similar to the amplitude based data at $\pm 1\%$.

8. Discussion and conclusion

This study has shown that absolute blood SO_2 can be obtained from photoacoustic spectra with an accuracy of better than 4% SO_2 for the amplitude based measurements (figure 8) and 2.5% SO_2 for the μ_{eff} based measurements (figure 9), and a resolution of $\pm 1\%$ in both cases. It was found that the resolution is predominately dependent upon the signal-to-noise ratio and that other error sources, such as the uncertainty in the specific absorption coefficients and the scattering efficiency, were negligible. From these results it can be concluded that the accuracy of this technique is comparable to that of the CO-oximeter. To achieve this high level of accuracy it is important (as figure 7 shows) that the wavelength dependence of scattering $\alpha_{scat}(\lambda)$ is incorporated into the forward model used to recover SO_2 from the measured photoacoustic spectrum, irrespective of the data type used. This is not especially problematic as $\alpha_{scat}(\lambda)$ can be readily measured or approximated to and is largely independent of the haematocrit, SO_2 and other physiological parameters. However, including $\alpha_{scat}(\lambda)$ brings an additional unknown, k, into the forward model. This requires obtaining photoacoustic signals at a minimum of three rather than two wavelengths as is often suggested (Esenaliev *et al* 2002, Savateeva *et al* 2002, Kiser *et al* 2004, Wang *et al* 2004) to obtain SO_2.

Although this study has shown that the photoacoustic amplitude spectrum can be used to obtain SO_2 with high accuracy and resolution, the measurement accuracy is strongly dependent upon a variety of amplitude scaling parameters such as the detector sensitivity or incident laser fluence. If any of these are unknown or cannot be measured accurately and therefore corrected for, the measured spectrum will be corrupted resulting in errors in the SO_2 measurement. By contrast the μ_{eff} spectrum is recovered from the shape of the photoacoustic signal and is therefore less sensitive to such influences. As a result, the under-reading of SO_2 exhibited by the amplitude based measurements is not in evidence. Whilst the ability to recover μ_{eff} by fitting a simple exponential function to the signal is only possible with the simple one-dimensional geometry used in this study, it does illustrate the clear advantage of using a data type that is characteristic of the shape of the signal where possible.

Although high accuracy and resolution has been obtained for all the measurements in this study, irrespective of the data type and the forward models used, it is instructive to examine the more general applicability of the different methods outlined. For the amplitude based SO_2 measurements, the approximation that the photoacoustic signal is proportional to the absorption coefficient, although based on little more than intuition, does allow reasonably accurate estimations of SO_2 to be made. The advantage of using a linear model such as this is that it involves solving a set of simultaneous linear equations and is therefore computationally efficient. However, its successful use is arguably little more than a fortuitous result arising from the very simple geometrical conditions and limited range of optical coefficients encountered in this study. It is unlikely to be readily extendable to a more complex and anatomically realistic geometry such as a vascular network located at depth in tissues containing spectrally significant chromophores. By contrast, the use of the iteratively applied diffusion based nonlinear forward model described in section 5.1.1 has a sounder theoretical basis enabling it

to be used with greater confidence and indeed it does appear to give greater accuracy than the linear forward model across the SO_2 range investigated. Furthermore, although an analytic solution of the diffusion equation for a specific geometry was used in this study, the use of a numerical solution (e.g. a finite element method (Arridge *et al* 1993)) would enable a forward model for arbitrary source geometries to be formulated. For example, discrete cylindrical absorbers immersed in turbid media of wavelength dependent optical coefficients representing a network of blood vessels could be modelled. Such a forward model could then be applied iteratively in the same way that the analytic solution described in section 5.1.1 was to recover SO_2.

In summary, the underlying methodology for measuring blood SO_2 from time-resolved photoacoustic signals has been established and the technique shown to be capable of providing an accuracy and resolution comparable to that of a CO-oximeter. Future work will focus on extending the techniques developed in this study to making spatially resolved measurement of blood SO_2.

Acknowledgments

This study was funded by the Engineering and Physical Sciences Research Council.

Appendix. δ-E(3) diffusion model

The starting point for describing the light transport in blood is the standard diffusion approximation to the radiative transfer equation for a collimated incident beam. This is given by

$$\nabla^2\Phi_s(\boldsymbol{r}) - 3\mu_a\mu_{tr}\Phi_s(\boldsymbol{r}) = -3\mu_s(\mu_{tr} + g\mu_t)E(\boldsymbol{r}), \tag{A.1}$$

where $\Phi_s(\boldsymbol{r})$ is the diffuse fluence rate at position $\boldsymbol{r}$. μ_a and μ_s are the absorption and scattering coefficients respectively, g is the anisotropy factor, the transport attenuation coefficient μ_{tr} is given by $\mu_{tr} = \mu_a + \mu_s'$ where μ_s' is the reduced scattering coefficient ($\mu_s' = \mu_s(1–g)$) and the total attenuation coefficient μ_t by $\mu_t = \mu_a + \mu_s$. The total fluence rate is the sum of $\Phi_s(\boldsymbol{r})$ and the irradiance source term $E(\boldsymbol{r})$. The latter represents the unscattered portion of the light due to the incident collimated beam propagating in the positive z direction and follows Beer's law.

$$E(\boldsymbol{r}) = E_0(x, y)\exp(-\mu_t z) \tag{A.2}$$

where $E_0(x, y)$ is the irradiance at the surface, assuming negligible refractive index mismatch.

For a large diameter collimated incident beam illuminating an infinite half space slab of homogeneous turbid media, an analytic solution to equation (A.1) that provides an expression for the depth dependent total fluence rate is available (Star 1995). In its standard form, this requires the usual assumption demanded by diffusion theory of near isotropic radiance. It is therefore of limited accuracy in describing the light distribution close to the surface (less than a few transport mean free paths) where the incident light remains highly directed—an accurate description in this region is required to model the peak amplitude of the photoacoustic signal which corresponds to the superficially absorbed optical energy. To address this limitation the solution is modified using an approach based upon consideration of a δ-Eddington phase function (Star 1995). This involves modifying the coefficients relating to scattering in the diffusion equation in such a way that a fraction f of the scattered light at shallow depths can be regarded as being shifted back into the collimated part of the beam. Fewer photons are therefore incorrectly transferred to the diffusive process close to the surface and the fluence rate is described more accurately in this region. Since only the coefficients relating to scattering

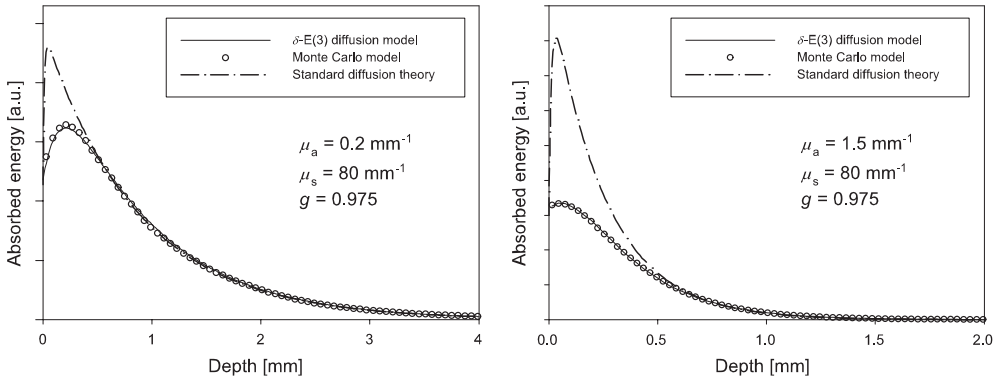

Figure 10. Comparison of the absorbed energy profiles obtained using a Monte Carlo model and the δ-E(3) diffusion model (equation (A.6)) for the minimum and maximum values of μ_a of blood of physiological haematocrit in the NIR. Similar levels of agreement were obtained for values of μ_a between these two extremes. For comparison purposes, the profiles obtained using standard diffusion theory ($f = 0$) are also shown. These illustrate the poor accuracy of this model close to the surface, particularly for the higher value of μ_a. The Monte Carlo model incorporated the refractive index mismatch between the cuvette window ($n = 1.5$) and blood ($n = 1.33$). The diameter of the incident collimated light was set to 6 mm.

are modified, the form of equation (A.1), and therefore any solution of it, remains unchanged. Implementation is thus achieved by a simple substitution of the modified coefficients.

The scattering coefficient, μ_s, is firstly modified by reducing it by a factor of $(1 - f)$ and denoted μ_{sE} thus,

$$\mu_{sE} = \mu_s(1 - f). \tag{A.3}$$

Since μ_s appears explicitly only in the source term of the diffusion equation (the right-hand side of equation (A.1)), modifying it in this way reduces the amount of light scattered out of the collimated incident beam as required. At greater depths, where z is sufficiently large that the contribution of the source term is negligible, the standard diffusion approximation is valid. Since scattering here is characterized solely (and accurately) by the reduced scattering coefficient μ_s' we require this parameter to remain unchanged. Thus,

$$\mu_{sE}' = \mu_{sE}(1 - g_E) = \mu_s' = \mu_s(1 - g), \tag{A.4}$$

where g_E is the modified version of g, the anisotropy factor. To fulfil the condition imposed by equation (A.4), g_E is given by

$$g_E = \frac{g - f}{1 - f}. \tag{A.5}$$

In essence, the reduction in μ_s given by equation (A.3) required to reduce the scattered component of the incident beam is compensated for by increasing $(1 - g)$. This is so that μ_s' is left unmodified in order that the solution reduces to that of the standard diffusion approximation at depths where the light is fully diffuse. This can be done because μ_s' appears explicitly only on the left-hand side of equation (A.1) (which describes the light diffusion in the far field) and g and μ_s appear explicitly only in the source term on the right-hand side.

The fraction f is obtained by matching the moments of the Legendre series expansion of the δ-Eddington phase function to those of the Henyey Greenstein phase function, the latter being widely used for biological tissues. For N expansion terms $f = g^N$. Following extensive comparison with Monte Carlo models (Wang *et al* 1995, 1997) (see figure 10) for the range

of optical coefficients likely to be encountered in this study, $N = 3$ was found to provide the greatest accuracy. Adopting the notation of Meador and Weaver (1979), this is termed the δ-E(3) approximation. The modified scattering related coefficients μ_{sE}, μ'_{sE} and g_E are now substituted into the analytic solution of equation (A.1) referred to above (Star 1995) to give the normalized total fluence $\Phi(z, \mu_a, \mu_s)$ as a function of depth z

$$\Phi(z, \mu_a, \mu_s) = \exp(-\mu_t z) + \frac{2}{\mu_t^2 - \mu_{eff}^2}[S_+(1+q)\exp(-\mu_{eff} z) - (S_+ + S_-)\exp(-\mu_t z)] \tag{A.6}$$

where the total attenuation coefficient μ_t is given by $\mu_t = \mu_a + \mu_{sE}$ and the effective attenuation coefficient $\mu_{eff} = (3\mu_a(\mu_a + \mu'_{sE}))^{1/2}$. S_+ and S_- are given by

$$S_+ = 0.25\mu_{sE}[(5 + 9g_E)\mu_a + 5\mu_{sE}] \tag{A.7}$$

and

$$S_- = 0.25\mu_{sE}[(1 - 3g_E)\mu_a + \mu_{sE}]. \tag{A.8}$$

q is given as

$$q = \frac{\mu_{eff} - 2\mu_a}{\mu_{eff} + 2\mu_a}. \tag{A.9}$$

The purpose of developing the above model of light transport was to be able to accurately describe the fluence close to the illuminated surface in order to be able to formulate an accurate forward model of the peak amplitude of the photoacoustic signal—one of the two spectroscopic data types used in this study. The other data type is μ_{eff} and is recovered by analysing the temporal characteristics of the part of the photoacoustic signal that has originated from depths greater than a few transport mean free paths. In this region, where the light is fully diffuse, equation (A.6) can be reduced to the familiar simple expression below,

$$\Phi(z, \mu_a, \mu_s) = D\exp(-\mu_{eff} z) \tag{A.10}$$

where D is a constant. As discussed in section 5.2, by substituting equation (A.10) into equation (2) and fitting the exponential function to the initial compressive part of the photoacoustic signal, μ_{eff} can be determined. Note that obtaining equation (A.10) usually requires $\mu_a \ll \mu'_s$, which is not strictly always the case for blood at certain near-infrared wavelengths and SO_2 values. However, it was found that fitting equation (A.10) to the results of the Monte Carlo model in order to determine μ_{eff} provided an agreement of better than 5% for the typical range of optical coefficients encountered in blood. Even for an extreme case of $\mu_a / \mu'_s \sim 1/2$, the agreement was within 10%.

References

Arridge S R, Schweiger M, Hiraoka M and Delpy D T 1993 A finite-element approach for modelling photon transport in tissue *Med. Phys.* **20** 299–309

Barlow R B and Polanyi M L 1962 Absorption measurements for oxygenated and reduced haemoglobin in range 0.6–1.88 microns *Clin. Chem.* **8** 67–74

Beard P C 2002 Photoacoustic imaging of blood vessel equivalent phantoms *Proc. SPIE* **4618** 54–62

Beard P C 2003 Interrogation of free-space Fabry–Perot sensing interferometers by angle tuning *Meas. Sci. Technol.* **14** 1998–2005

Beard P C, Perennes F and Mills T N 1999 Transduction mechanisms of the Fabry–Perot polymer film sensing concept for wideband ultrasound detection *IEEE Trans. Ultrason. Ferroelectr. Freq. Control* **46** 1575–82

Bessman J D and Johnson R K 1975 Erythrocyte volume distribution in normal and abnormal subjects *Blood* **46** 369–79

Cope M 1991 The application of near infrared spectroscopy to noninvasive monitoring of cerebral oxygenation in the newborn infant *PhD Thesis* University College, London

Enejder A M K, Swartling J, Aruna P and Andersson-Engels S 2003 Influence of cell shape and aggregate formation on the optical properties of flowing whole blood *Appl. Opt* **42** 1384–94

Esenaliev R O, Larina I V, Larin K V, Deyo D J, Motamedi M and Prough D S 2002 Optoacoustic technique for noninvasive monitoring of blood oxygenation: a feasibility study *Appl. Opt.* **41** 4722–31

Fainchtein R, Stoyanov B J, Murphy J C, Wilson D A and Hanley D F 2000 Local determination of hemoglobin concentration and degree of oxygenation in tissue by pulsed photoacoustic spectroscopy *Proc. SPIE* **3916** 19–33

Geigy J R 1956 *Documenta Geigy Scientific Tables* vol 5 (Basle: Jesse Broad)

Hale G M and Querry M R 1973 Optical constants of water in 200 nm to 200 μm wavelength region *Appl. Opt.* **12** 555–63

Hammer M, Schweitzer D, Michel B, Thamm E and Kolb A 1998 Single scattering by red blood cells *Appl. Opt.* **37** 7410–8

Horecker B L 1943 The absorption spectra of hemoglobin and its derivatives in the visible and near-infrared regions *J. Biol. Chem.* **148** 173–83

Kiser W L, Kruger R A, Reinecke D, Kruger G and Miller K D 2004 Thermoacoustic in-vivo determination of blood oxygenation *Proc. SPIE* **5320** 1–7

Kolkman R G M, Hondebrink E, Steenbergen W and de Mul F F M 2003 In-vivo photoacoustic imaging of blood vessels using an extreme-narrow aperture sensor *IEEE J. Select. Top. Quantum Electron.* **9** 343–6

Laufer J, Elwell C, Delpy D and Beard P 2004 Pulsed near-infrared photoacoustic spectroscopy of blood *Proc. SPIE* **5320** 57–68

Meador W E and Weaver W R 1979 Diffusion approximation for large absorption in radiative transfer *Appl. Opt.* **18** 1204–8

Paltauf G, Kostli K P, Frauchiger D and Frenz M 2001 Spectral optoacoustic imaging using a scanning transducer *Proc. SPIE* **4434** 81–8

Roggan A, Friebel M, Dorschel K, Hahn A and Muller G 1999 Optical properties of circulating human blood in the wavelength range 400–2500 nm *J. Biomed. Opt.* **4** 36–46

Savateeva E V, Karabutov A A, Solomatin S V and Oraevsky A A 2002 Optical properties of blood at various levels of oxygenation studied by time resolved detection of laser-induced pressure profiles *Proc. SPIE* **4618** 63–75

Star W M 1995 Diffusion theory of light transport *Optical-thermal Response of Laser-irradiated Tissue* ed A J Welch and M J C van Gemert (New York: Plenum) chapter 6, pp 131–206

Steinke J M and Shepherd A P 1988 Comparison of Mie theory and the light-scattering of red blood cells *Appl. Opt.* **27** 4027–33

Takatani S and Graham M D 1979 Theoretical analysis of diffuse reflectance from a 2-layer tissue model *IEEE Trans. Biomed. Eng.* **26** 656–64

Wang L H, Jacques S L and Zheng L Q 1995 MCML—Monte Carlo modeling of photon transport in multi-layered tissues *Comput. Methods Programs Biomed.* **47** 131–46

Wang L H, Jacques S L and Zheng L Q 1997 CONV—convolution for responses to a finite diameter photon beam incident on multi-layered tissues *Comput. Methods Programs Biomed.* **54** 141–50

Wang X D, Ku G, Xie X Y, Wang Y W, Stoica G and Wang L V 2004 Non-invasive functional photoacoustic tomography of blood oxygen saturation in the brain *Proc. SPIE* **5320** 69–76

Wang X D, Pang Y J, Ku G, Xie X Y, Stoica G and Wang L H V 2003 Non-invasive laser-induced photoacoustic tomography for structural and functional in vivo imaging of the brain *Nature Biotechnol.* **21** 803–6

Wray S, Cope M, Delpy D T, Wyatt J S and Reynolds E O R 1988 Characterization of the near-infrared absorption spectra of cytochrome-AA3 and haemoglobin for the non-invasive monitoring of cerebral oxygenation *Biochim. Biophys Acta* **933** 184–92